Supporting Information

A dipicolinic acid tag for rigid lanthanide tagging of proteins and paramagnetic NMR spectroscopy

Xun-Cheng Su, Bradley Man, Sophie Beeren, Haobo Liang, Shane Simonsen, Christophe Schmitz, Thomas Huber, Barbara A. Messerle, and Gottfried Otting

Synthesis of 4-Mercaptomethyl-2,6-pyridine dicarboxylic acid

General Procedures

Dipicolinic acid and *p*-toluenesulfonyl chloride were purchased from Aldrich and used as received. The compounds 2,6-dimethoxycarbonyl-4-hydroxymethylpyridine and 2,6-dimethoxycarbonyl-4-tosyloxymethylpyridine were prepared by modified literature methods (Shelkov and Melman, 2005; Tang *et al.* 2006). Bulk compressed nitrogen (>99.5%) was obtained from Linde Gas Pty and used as supplied.

Melting points were determined using a Gallenkamp melting point apparatus and are uncorrected.

^{1}H and $^{13}C\{^{1}H\}$ NMR spectra were recorded on either a Bruker DPX300 spectrometer operating at 300 MHz (^{1}H), 75 MHz (^{13}C) or a Bruker Avance 800 spectrometer operating at 800 MHz (^{1}H), 201 MHz (^{13}C). Chemical shifts were internally referenced to the residual solvent peaks and all spectra were recorded at 298 K unless otherwise stated. ^{1}H-^{13}C HMBC and ^{1}H-^{13}C HSQC spectra were used for the assignment of organic compounds.

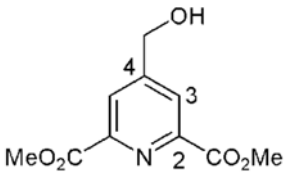

2,6-Dimethoxycarbonyl-4-hydroxymethylpyridine (1). This compound was prepared following the general procedure of Tang *et al.* (2006) and was identified by comparison of literature NMR data.

To a round bottom flask containing a solution of sulfuric acid (30% v/v, 30 ml) and methanol (30 ml) was added 2,6-dimethoxycarbonylpyridine (5.61 g, 28.7 mmol). The resulting suspension was cooled to room temperature using an ice bath and hydrogen peroxide (30% v/v, 24 ml, 210 mmol) and a saturated aqueous solution of ferrous sulfate (30 ml) were added dropwise maintaining the temperature between 20 – 25 ºC. After the addition was complete, the solution was stirred for an additional 20 min at room temperature. Potassium carbonate was added until the solution reached neutral pH whereupon the resulting suspension was filtered. The filtrate was extracted with ethyl acetate (4 x 50 ml), the organic phase dried over sodium sulfate, filtered, and the solvent was removed *in vacuo* to yield the crude product as a beige solid. The latter was purified using column chromatography (SiO_2, 100% chloroform) to yield

the titled compound as a white solid (1.22 g, 19%).

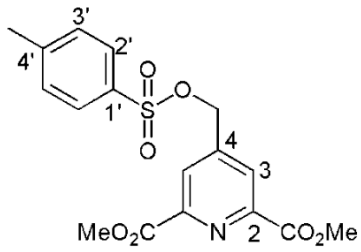

2,6-Dimethoxycarbonyl-4-tosyloxymethylpyridine (2). This compound was prepared following the general procedure of Tang *et al.* and was identified by comparison of literature NMR data.

To a cooled solution of 2,6-dimethoxycarbonyl-4-hydroxymethylpyridine (**1**) (2.15 g, 9.56 mmol) in dichloromethane (20 ml) was added dropwise a solution of tosyl chloride (2.37 g, 8.92 mmol) in dichloromethane (10 ml). The resulting solution was stirred for 20 min at 0 ^{o}C whereupon triethylamine (6 ml) was added dropwise in three portions at 20 min intervals. After the addition was complete, the solution was stirred at 0 ^{o}C for an additional 15 min, followed by 15 min at room temperature. The resulting dark solution was diluted with ethyl acetate (40 ml), washed with water (2 x 20 ml) and 3 M hydrochloric acid (2 x 20 ml). The organic phase was dried over calcium chloride, filtered, and the solvent removed *in vacuo* to yield a brown powder, which was washed with diethyl ether (3 x 10 ml) to yield the titled compound as a tan solid (2.96 g, 82%) that was used without further purification.

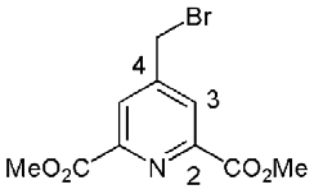

2,6-Dimethoxycarbonyl-4-bromomethylpyridine (3).

Lithium bromide (212 mg, 2.44 mmol) was added to a solution of dimethoxycarbonyl-4-tosyloxymethylpyridine (**2**) (460 mg, 1.22 mmol) in acetone (25 ml) and stirred at room temperature for 2 hours. The resulting suspension was filtered, concentrated *in vacuo* and the residues triturated with chloroform (50 ml). The solvent was removed *in vacuo* to yield the titled compound as a tan solid (233 mg, 67%) that was used without further purification.

Mp: 110-114 ^{o}C.

^{1}H NMR (300 MHz, $CDCl_3$) δ 8.31 (s, 2H, **H3**), 4.50 (s, 2H, C**H**$_2$Br), 4.03 (s, 6H, CO_2C**H**$_3$).
^{13}C{^{1}H} NMR (75 MHz, $CDCl_3$) δ 164.6 (**C**O_2CH_3), 149.2 (**C2**), 148.9 (**C4**), 127 (**C3**), 53.3 (CO_2**C**H_3), 29.3 (**C**H_2Br).

Anal. Calcd. $C_{10}H_{10}NO_4Br$: C, 41.62; H, 3.50; N, 4.86;
Found: C, 41.69; H, 3.55; N, 4.76.

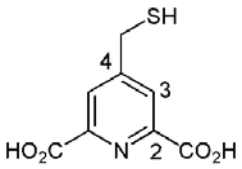

4-Mercaptomethyl-2,6-pyridinedicarboxylic acid (4).

Under a nitrogen atmosphere, a solution of (**3**) (190 mg, 0.662 mmol) and thiourea (58.8 mg, 0.772 mmol) in methanol (10 ml) was refluxed overnight. The solution was allowed to cool to room temperature and the solvent was removed *in vacuo*. The resulting residue was dissolved in deoxygenated water (20 ml), and sodium hydroxide pellets (190 mg, 4.75 mmol) added. The mixture was refluxed overnight under a nitrogen atmosphere. The solution was eluted through a cation exchange resin column (Amberlite GC120) and the solvent removed *in vacuo* to yield the titled compound (**4**) as a tan solid (130 mg, 99%).

Mp: >150 ^{o}C (dec)

^{1}H NMR (800 MHz, D_2O) δ 8.28 (s, 2H, **H3)**, 3.86 (s, 2H, C**H**$_2$SH). ^{13}C{^{1}H} NMR (201 MHz, D_2O) δ 171.6 (**C**O_2H), 153.0 (**C2**), 152.3 (**C4**), 124.2 (**C3**), 26.8 (**C**H_2SH).

EI-HRMS Calcd. for $C_8H_7NO_4S$ $[M-H]^-$: 212.0096. Found 212.0016.

References

Shelkov, R.; Melman, A. *Eur. J. Org. Chem.* **2005**, 1397-1401.
Tang, R.; Zhao, Q.; Yan, Z.; Luo, Y. *Synth. Commun.* **2006**, 36, 2027-2034.

Ligation of 4MMDPA to ArgN

All steps were performed at room temperature. The ArgN protein (0.5 ml of a 1 mM solution per NMR sample) was first reduced with 5 equivalents of DTT at pH 7.0. Free DTT was washed out completely using reaction buffer (50 mM Tris, pH 7.6) and a Millipore ultrafilter with a MW cutoff of 5 kD. The final volume was about 1 ml. 20 equivalents of 5, 5'-dithiobis-(2-nitrobenzoic acid) (DTNB) were dissolved in 5 ml reaction buffer and the pH adjusted to 7.6. The protein was added stepwise into the DTNB solution and the solution mixed well after each addition. The reaction generates yellow thionitrobenzoate. Subsequently, the protein solution was left at room temperature for 1 hour. The mixture of activated protein, excess DTNB and thionitrobenzoate was concentrated to 0.3 ml and washed with reaction buffer about 4 times (corresponding to 8,000-fold dilution), resulting in a colorless solution.
5 equivalents of 4-mercaptomethyl-dipicolinic acid (4MMDPA) were weighed and dissolved in 1.5 ml reaction buffer. The 4MMDPA solution was poured into the solution containing the activated protein. The reaction of 4MMDPA with the activated protein releases yellow thionitrobenzoate. The solution was left at room temperature for 1 hour and subsequently concentrated and washed with reaction buffer. The ArgN-4MMDPA product was purified by FPLC using a MonoQ column. The overall yield was about 85%.

NMR measurements

All NMR measurements were performed at 25 ^{o}C in solutions containing 20 mM 2-(*N*-morpholino)ethanesulfonic acid (MES) buffer at pH 6.5, using a Bruker 800 MHz NMR spectrometer equipped with a cryoprobe. Residual dipolar couplings were measured in the ^{15}N dimension of ^{15}N-HSQC spectra recorded with the IPAP scheme (Ottiger, M.; Delagio, F.; Bax, A. *J. Magn. Reson.* **1998**, 131, 373-378), using t_{1max} values of 70 ms.

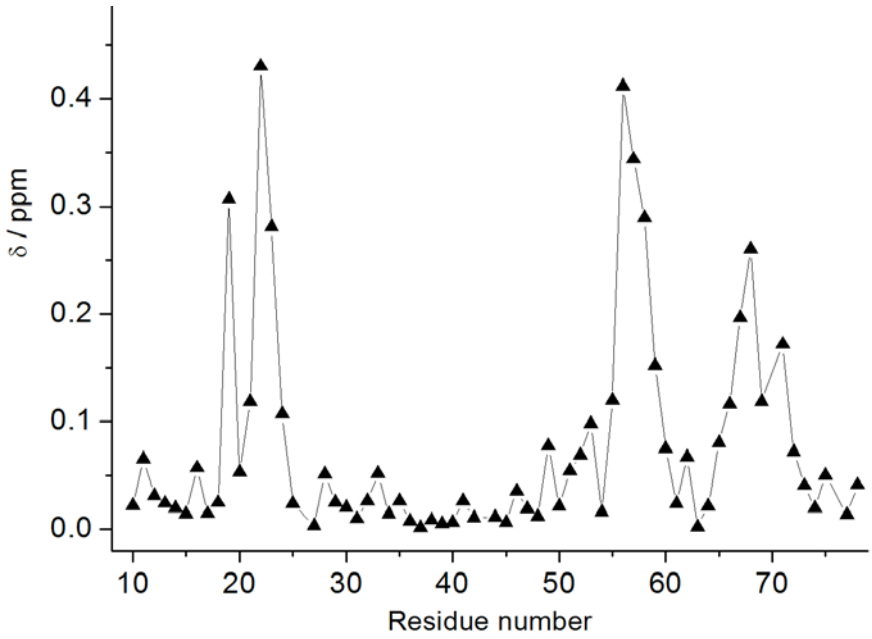

Figure S1. Chemical shift difference δ of backbone amides of ArgN, comparing underivatized ArgN and the ArgN-4MMDPA-Lu^{3+} complex. Solution conditions: 25 ^{o}C, pH 6.5 in 20 mM MES buffer. δ was calculated as $\delta = \sqrt{(\delta^{15}N/10)^2 + (\delta^{1}H)^2}$, where $\delta^{15}N$ and $\delta^{1}H$, respectively, are the chemical shift differences measured in the ^{15}N and ^{1}H dimensions of the ^{15}N-HSQC spectra. All chemical shift changes with δ > 0.2 ppm involve amide protons within 6.5 Å of Cys68 C^{α}, showing that the 4MMDPA tag changes the chemical environment only locally without causing long-range structural disturbance. Chemical shift changes caused by the additional presence of Lu^{3+} were much smaller, with the largest amide chemical shift change observed for Glu21 (Figure S2).

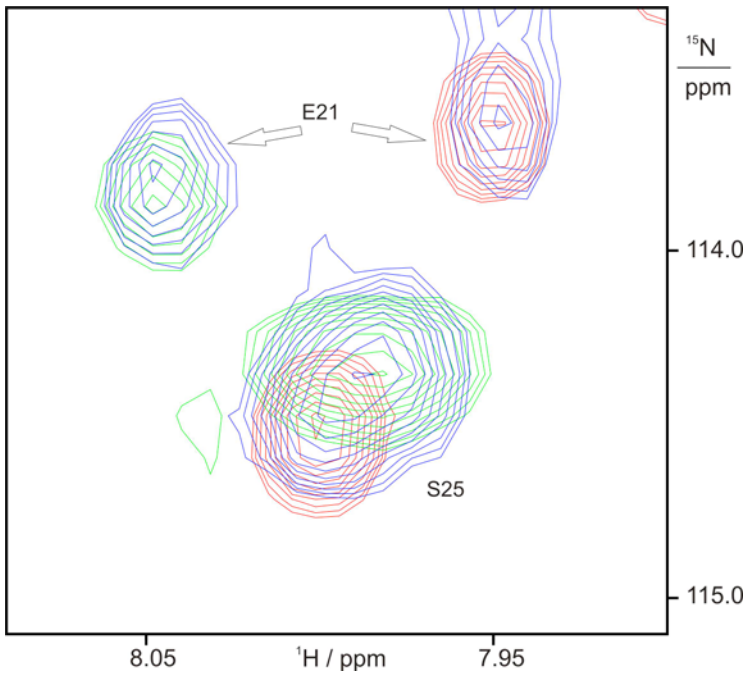

Figure S2. Superimposition of ^{15}N-HSQC spectra of uniformly ^{15}N-labeled ArgN-4MMDPA-Lu^{3+} complex (red), and ArgN-4MMDPA in the presence of $[Lu(DPA)]^{+}$ (blue), or $[Lu(DPA)_2]^{-}$ (green). The molar ratio of [total Lu^{3+}]:[protein] was 1.5:1. Only the spectral region containing the cross-peaks of Glu21 and Ser25 is shown. Glu21 is one of the residues with the largest amide chemical shift changes between the ArgN-4MMDPA-Lu^{3+} complex and the sample containing $[Lu(DPA)_2]^{-}$.

We interpret the data as follows. *Red spectrum:* $LuCl_3$ quantitatively forms the ArgN-4MMDPA-Lu^{3+} complex. *Green spectrum:* The affinity of ArgN-4MMDPA for Lu^{3+} is insufficient to compete with DPA, if the concentration of DPA in the solution is two-fold higher than that of Lu^{3+}. This conclusion is confirmed by the fact that a ^{15}N-HSQC spectrum of ArgN-4MMDPA in the presence of a 1:1 mixture of $[Lu(DPA)_2]^{-}$ and $[Yb(DPA)_2]^{-}$ did not show paramagnetic shifts (data not shown). We could not confirm, however, that this spectrum represents the apo-ArgN-4MMDPA construct, because the ^{15}N-HSQC spectrum of ArgN-4MMDPA in the absence of any lanthanide, although showing very similar chemical shifts as the green spectrum, was affected by severe line broadening, particularly in the vicinity of Cys68, and peak doubling for some of the amides, indicating conformational heterogeneity introduced by the tag (data not shown). *Blue spectrum:* This spectrum shows that the affinity of ArgN-4MMDPA for Lu^{3+} is sufficient to compete with DPA as it contains all the cross-peaks of the ArgN-4MMDPA-Lu^{3+} complex. Each peak is doubled by the simultaneous presence of apo-ArgN-4MMDPA as observed in the green spectrum.

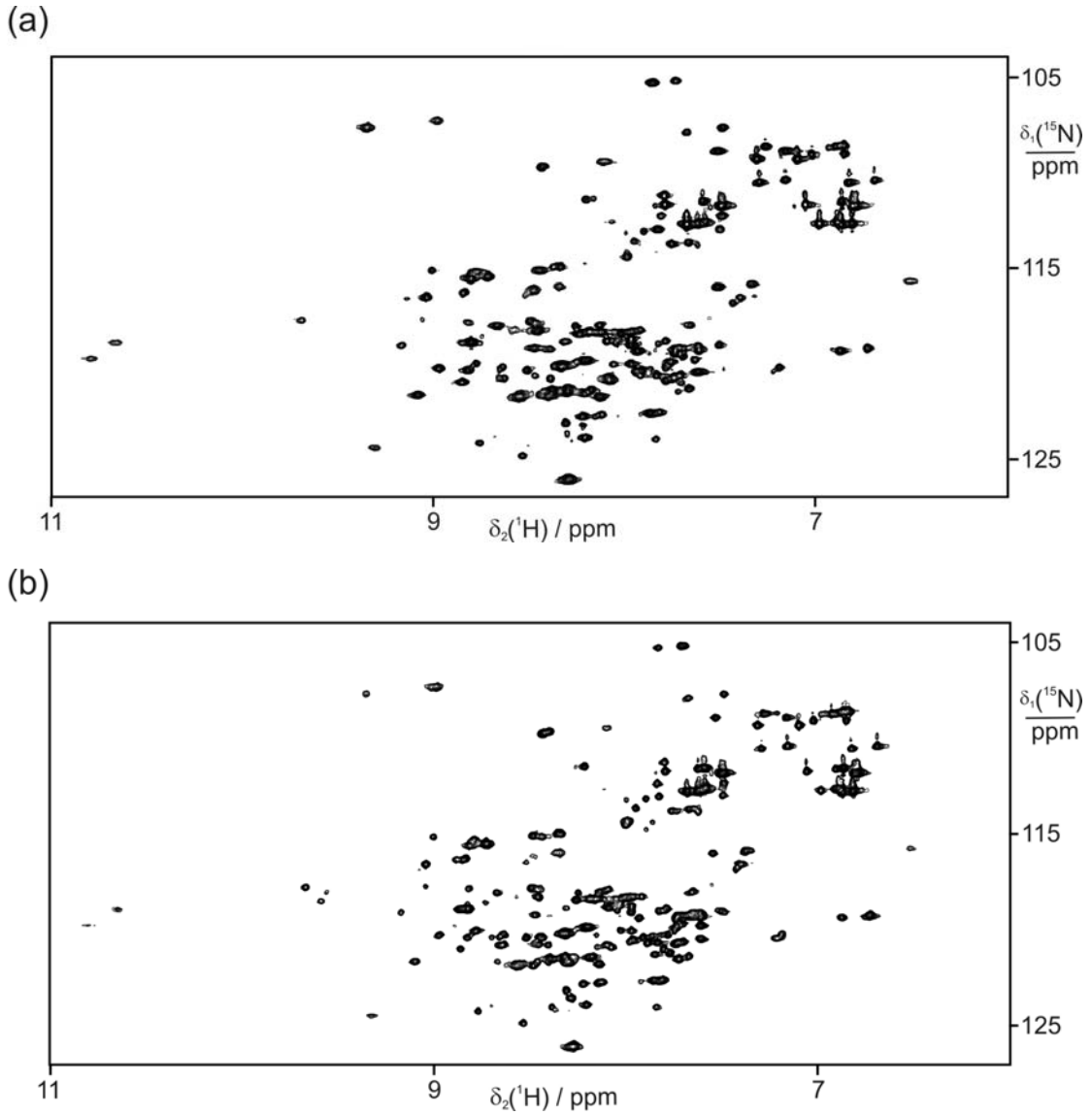

Figure S3. ^{15}N-HSQC spectra of ^{15}N-ArgN-4MMDPA with a 1:1 mixture of Lu^{3+} and Yb^{3+} (a), or a 1:1 mixture of $[LuDPA]^{+}$ and $[YbDPA]^{+}$ (b). The molar ratio of [total Ln^{3+}]:[protein] was 1.5:1. The conservation of chemical shifts in the diamagnetic and paramagnetic states indicates that the ArgN-4MMDPA-Ln^{3+} complexes cannot bind additional DPA.

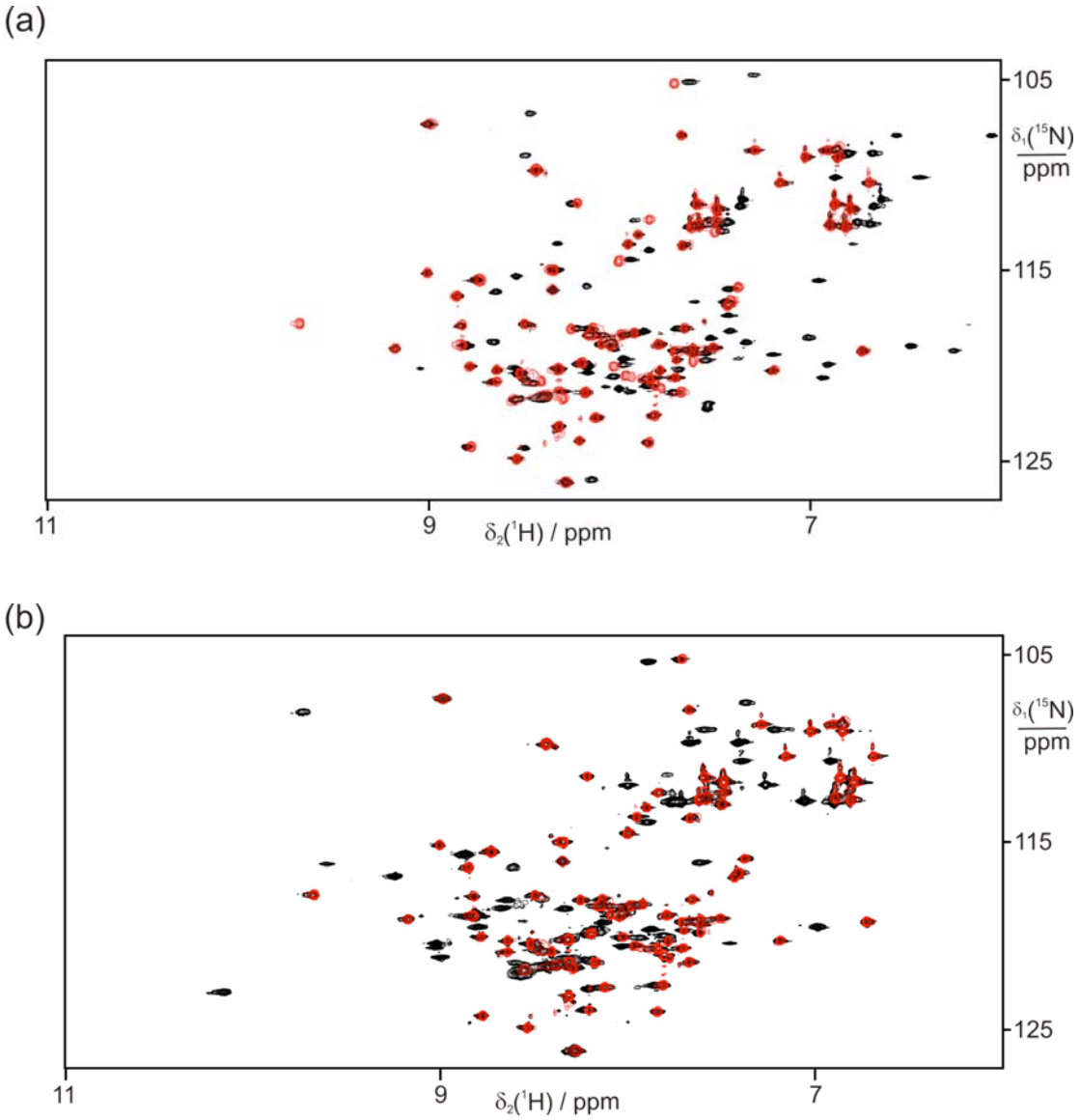

Figure S4. NMR spectra used for the measurement of PCS. (a) Superimposition of ^{15}N-HSQC spectra of uniformly ^{15}N-labeled ArgN-4MMDPA in the presence of a 1:1 mixture of Lu^{3+} and Tb^{3+} (black) and in the presence of Lu^{3+} (red). (b) Superimposition of ^{15}N-HSQC spectra of uniformly ^{15}N-labeled ArgN-4MMDPA in the presence of a 1:1 mixture of Lu^{3+} and Tm^{3+} (black) and in the presence of Lu^{3+} (red). The ratio of lanthanides to protein was about 1.5:1.

Table S1. ^{15}N and $^{1}H^{N}$ chemical shifts of ArgN-4MMDPA complexed with Lu^{3+}, Tb^{3+}, Tm^{3+}, and Yb^{3+} in 20 mM MES (pH 6.5) at 25 ^{o}C and a ^{1}H NMR frequency of 800 MHz.

	Lu^{3+}		Tb^{3+}		Tm^{3+}		Yb^{3+}	
Assignment	δ^{N} /ppm	δ^{H} /ppm	δ^{N} /ppm	δ^{H} /ppm	δ^{N} /ppm	δ^{H} /ppm	δ^{N} /ppm	δ^{H} /ppm
A5N-HN	126.1	8.27	126.0	8.14	126.1	8.27	126.1	8.30
K6N-HN	120.2	8.31	120.0	8.16	120.1	8.32	120.2	8.33
7NE2-HE21	111.8	7.48	111.7	7.36	111.8	7.49	111.8	7.50
7NE2-HE22	111.8	6.78	111.7	6.66	111.8	6.79	111.8	6.81
Q7N-HN	120.8	8.41			120.8	8.41	120.9	8.39
E8N-HN	118.9	8.82	118.7	8.65	118.9	8.82	118.9	8.81
E9N-HN	119.9	8.19	119.6	7.98	119.9	8.19	119.9	8.22
L10N-HN	122.6	7.81	122.3	7.54	122.6	7.86	122.7	7.87
V11N-HN	118.4	7.99	118.1	7.70	118.4	8.00	118.5	8.02
K12N-HN	119.2	7.71	118.8	7.33	119.2	7.67	119.3	7.74
A13N-HN	122.7	8.12	122.0	7.53	122.8	8.21	122.8	8.22
F14N-HN	120.0	8.78	119.1	8.02	120.4	9.02	120.3	8.98
K15N-HN	117.8	8.50	116.6	7.60	118.1	8.65	118.1	8.67
A16N-HN	119.7	7.70	117.8	6.17	120.1	7.94	120.1	8.06
L17N-HN	118.0	7.66			119.2	8.55	118.9	8.31
L18N-HN	119.0	7.51						
K19N-HN	118.3	7.92						
E20N-HN	116.8	7.43						
E21N-HN	113.6	7.95						
K22N-HN	113.0	7.50						
F23N-HN	120.0	8.03						
S24N-HN	117.8	9.67					118.9	10.66
S25N-HN	114.5	8.00	113.6	6.78	116.2	9.61	115.3	8.78
26NE2-HE21	109.0	7.02	108.8	6.80	109.7	7.67	109.3	7.31
26NE2-HE22	109.1	6.85	108.9	6.67	109.7	7.41	109.3	7.10
G27N-HN	107.3	8.99	106.8	8.46	108.1	9.73	107.7	9.35
E28N-HN	121.4	7.67	120.6	6.93	122.2	8.57	121.8	8.13
I29N-HN	120.2	7.19	119.2	6.24	121.2	8.22	120.8	7.74
V30N-HN	118.9	8.09	118.2	7.42	119.5	8.79	119.2	8.48
A31N-HN	119.1	7.62	118.5	7.01	119.6	8.18	119.4	7.94
A32N-HN	120.6	7.70	119.9	6.91	121.1	8.33	120.9	8.09
L33N-HN	118.0	8.14	117.4	7.43	118.5	8.67	118.3	8.46
34NE2-HE21	110.4	7.16	110.1	6.87	110.6	7.39	110.6	7.30
34NE2-HE22	110.5	6.69	110.1	6.42	110.6	6.92	110.6	6.83
Q34N-HN	120.8	8.64	120.4	8.16	121.1	9.00	121.0	8.85
E35N-HN	121.7	8.29	121.1	7.85	121.9	8.57	121.8	8.41
36NE2-HE21	108.7	7.28	108.0	6.55	109.0	7.59	108.9	7.52
36NE2-HE22	108.7	6.90	108.0	6.05	109.0	7.22	108.9	7.16
Q36N-HN	115.9	7.37	115.6	6.95	116.1	7.62	116.0	7.52
G37N-HN	105.2	7.71	104.7	7.29	105.3	7.89	105.3	7.86
F38N-HN	119.8	7.61	119.4	7.19	119.9	7.81	120.0	7.77
D39N-HN	121.4	8.31	121.1	8.07	121.5	8.44	121.4	8.38
40ND2-HD21	112.7	7.62	112.6	7.49	112.9	7.72	112.8	7.68
40ND2-HD22	112.7	6.81	112.6	6.68	112.9	6.90	112.8	6.87
N40N-HN	115.5	8.73	115.3	8.54	115.7	8.87	115.6	8.81
I41N-HN	118.3	8.13	118.2	7.87	118.5	8.33	118.5	8.24
42ND2-HD21	112.6	6.89	112.5	6.75	112.8	7.06	112.7	6.98
42ND2-HD21	112.6	7.58	112.5	7.43	112.8	7.75	112.7	7.62
N42N-HN	119.2	6.73	118.9	6.47	119.5	6.99	119.4	6.88
43NE2-HE21	111.5	7.60	111.3	7.35	111.9	8.00	111.7	7.79

43NE2-HE22	111.6	6.87	111.3	6.63	111.9	7.27	111.7	7.06
S44N-HN	116.0	8.34	115.8	8.17	116.3	8.61	116.2	8.48
K45N-HN	121.4	8.18	121.2	8.00	121.7	8.42	121.5	8.30
V46N-HN	118.9	7.79	118.6	7.52	119.3	8.14	119.1	7.97
S47N-HN	116.4	8.85	116.1	8.64	116.8	9.24	116.6	9.04
R48N-HN	119.3	7.61	119.3	7.54	119.6	7.88	119.5	7.74
M49N-HN	120.2	7.78	120.2	7.68	120.5	8.03	120.4	7.92
L50N-HN	120.3	8.64	120.1	8.54	120.6	9.02	120.4	8.83
T51N-HN	113.7	7.67	114.0	7.84	113.9	7.90	113.8	7.76
K52N-HN	123.9	8.21	124.3	8.49	123.9	8.23	123.9	8.21
F53N-HN	113.2	7.90	113.6	8.32	112.9	7.77	113.0	7.83
G54N-HN	107.9	7.67	109.0	8.49	107.5	7.37	107.7	7.49
A55N-HN	118.9	8.05	120.1	9.04			118.8	7.97
V56N-HN	118.4	8.16					118.4	8.12
R57N-HN	118.8	8.04					119.3	8.40
T58N-HN	119.1	9.17					120.6	11.16
R59N-HN	124.0	7.84						
60ND2-HD21	112.3	7.49						
60ND2-HD22	112.4	7.84						
N60N-HN	124.2	8.77					124.5	9.31
A61N-HN	120.7	8.47						
K62N-HN	116.6	7.41					115.7	6.51
M63N-HN	111.5	8.22					111.3	7.80
E64N-HN	120.5	7.96						
M65N-HN	121.6	8.38			123.0	10.15	121.7	9.09
V66N-HN	117.9	8.82					119.8	10.80
Y67N-HN	118.1	8.25						
C68N-HN	115.2	9.00						
L69N-HN	121.8	8.55						
A71N-HN	124.9	8.53						
E72N-HN	120.4	8.52						
L73N-HN	123.2	8.31						
G74N-HN	109.8	8.44					109.5	8.11
V75N-HN	120.7	7.84						
T77N-HN	115.0	8.34						
T78N-HN	121.0	7.81						

Table S2. RDCs of backbone amides of ArgN-4MMDPA with Tb^{3+}, Tm^{3+} and Yb^{3+} [a]

Residue	Tb^{3+} / Hz	Tm^{3+} / Hz	Yb^{3+} / Hz
A5	-4.8		
K6	-0.1		
E8	-1.9		
E9	-5.8		
L10	-1.2	-1.1	-0.9
V11	-0.3	-4.8	-2.6
K12	-4.4	-0.5	
A13	-2.7	0.2	0.3
F14	-1.8	-3.9	-3.1
K15	-2.0	-3.6	-2.0
A16		-0.8	0.6
L17			-0.2
S25	4.5		-2.0
G27	-0.6	-0.8	-0.4
E28	-0.7		-1.3
I29	5.8		-2.0
V30	0.5	-0.8	-1.8
A31	-2.4	-1.0	-0.2
A32	2.5	-4.0	-1.9
L33	4.0	-1.0	-0.9
Q34	-0.3	-1.9	-1.5
E35	2.1	-2.5	-2.1
Q36	6.5	-4.9	-3.0
G37	-3.6	1.2	0.1
F38	-2.6	-2.3	-1.2
D39	-1.5		-1.2
N40	-3.9	4.3	1.4
I41	0.6	-6.6	-2.7
N42	-2.2	-0.4	-0.2
K45	-3.5	4.5	1.6
V46	-7.5	5.9	3.6
S47	-8.6	9.9	5.8
R48	-7.5	5.1	2.6
M49	-5.0	2.8	2.5
L50	-9.3	10.4	5.3
T51	-10.0	12.7	5.2
K52	-7.4		
F53	-5.2	4.9	3.1
G54	-3.6	7.1	3.1
A55	-5.8	0.0	3.6
V56			-0.5
R57			-0.7
T58			3.2
N60			6.3
K62			-1.9
M63			-2.2
M65			4.9
V66			4.9

[a] RDCs measured as the splitting observed for the Lu^{3+} complex minus the splitting observed for the Ln^{3+} complex at 25 ^{o}C and a ^{1}H NMR frequency of 800 MHz.

Table S3. Comparison of alignment tensor and Δχ-tensor parameters of ArgN-4MMDPA complexed with Tb^{3+}, Tm^{3+}, and Yb^{3+}, respectively.[a]

Ln^{3+}	$10^4 A_{ax}$[b]	$10^4 A_{rh}$[b]	$\Delta\chi_{ax}$[c]	$\Delta\chi_{rh}$[c]	$\Delta\chi_{ax}$[d]	$\Delta\chi_{rh}$[d]
Tb^{3+}	4.9±0.1	2.6±0.2	10.8	5.8	12.9±0.9	6.3±0.8
Tm^{3+}	5.6±0.2	2.8±0.2	12.2	6.1	12.2±0.6	6.9±0.8
Yb^{3+}	2.8±0.1	1.1±0.1	6.2	3.4	5.7±0.4	3.8±0.8

[a] All data recorded at 25 °C and 800 MHz ^{1}H NMR frequency. The tensor parameters were obtained as averages of independent fits performed for each of the 23 NMR conformers of the ArgN structure (Sunnerhagen *et al*., 1997).

[b] Alignment tensor determined using Pales (Zweckstetter and Bax, 2000). Only RDCs of residues in regular secondary structure elements were used in the fit (residues 10-17, 28-34, 45-52). Our definition of the alignment matrix **A** follows that of Kramer *et al.* (2004), *i.e*. **A** = 2/3 **S**, where **S** is the Saupe matrix for a liquid crystal with an optical axis collinear with the direction of the magnetic field. For consistency with these definitions, the values A_a and A_{rh} listed in the table are two times larger than those reported by Pales as Da and Dr. The program Module (Dosset *et al*., 2001) also reports Da and Dr values two times larger than Pales. The RDCs used for the fits are indicated in Table S2.

[c] Δχ-tensor parameters (in units of 10^{-32} m^3) obtained from A_{ax} and A_{rh} values using

$$\Delta\chi_{ax,rh} = \frac{15kT\mu_0}{B_0^2} A_{ax,rh}$$

[d] Δχ-tensor parameters (in units of 10^{-32} m^3) determined by the program Numbat (Schmitz *et al*., 2008). The tensor parameters were obtained by simultaneously fitting the PCS data of all 3 lanthanides to yield the 3 different tensors with a single common metal ion position. Only the PCS measured for backbone amide protons of ArgN-4MMDPA of residues 10-66 were used in the fits. For comparison with the alignment tensor, the biggest positive principal axis was defined as the z-axis and the smallest principal axis was defined as the x-axis.

Dosset, P.; Hus, J.-C.; Marion, D.; Blackledge, M. *J. Biomol. NMR* **2004**, 20, 223-231.

Kramer, F.; Deshmukh, M. V.; Kessler, H.; Glaser, S. J. *Concepts Magn. Reson*. **2004**, 21A, 10-21.

Schmitz, C.; Stanton-Cook, M. J.; Su, X.-C.; Otting, G.; Huber, T. *J. Biomol. NMR* **2008**, 41, 179-189.

Sunnerhagen, M.; Nilges, M.; Otting, G.; Carey, J. *Nat. Struct. Biol*. **1997**, 4, 819-826.

Zweckstetter, M.; Bax, A. *J. Am. Chem. Soc*. **2000**, 122, 3791-3792.

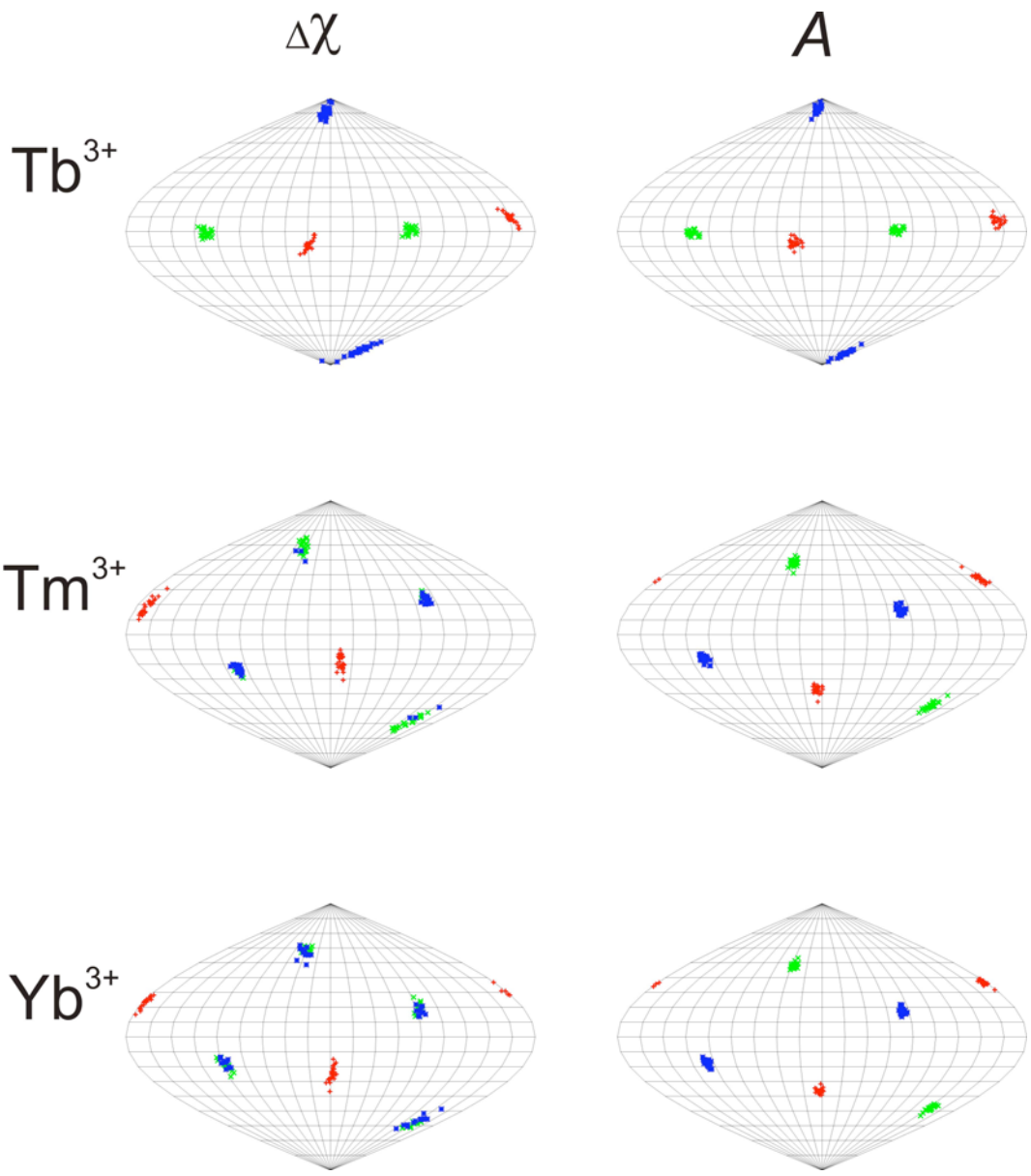

Figure S5. Sanson-Flamsteed projection plots comparing the orientations of the principal axes of the Δχ-tensors (left panel) and alignment tensors (right panel) determined for the 23 NMR conformers of the ArgN structure as described in Table S3. The plots show the points where the principal axes penetrate the sphere, with the z-, y-, and x-axis in blue, green, and red, respectively. The convention |z| > |y| > |x| was used to name the axes, resulting in occasional swaps between the z- and y-axes of the Δχ-tensors when their magnitudes were similar.

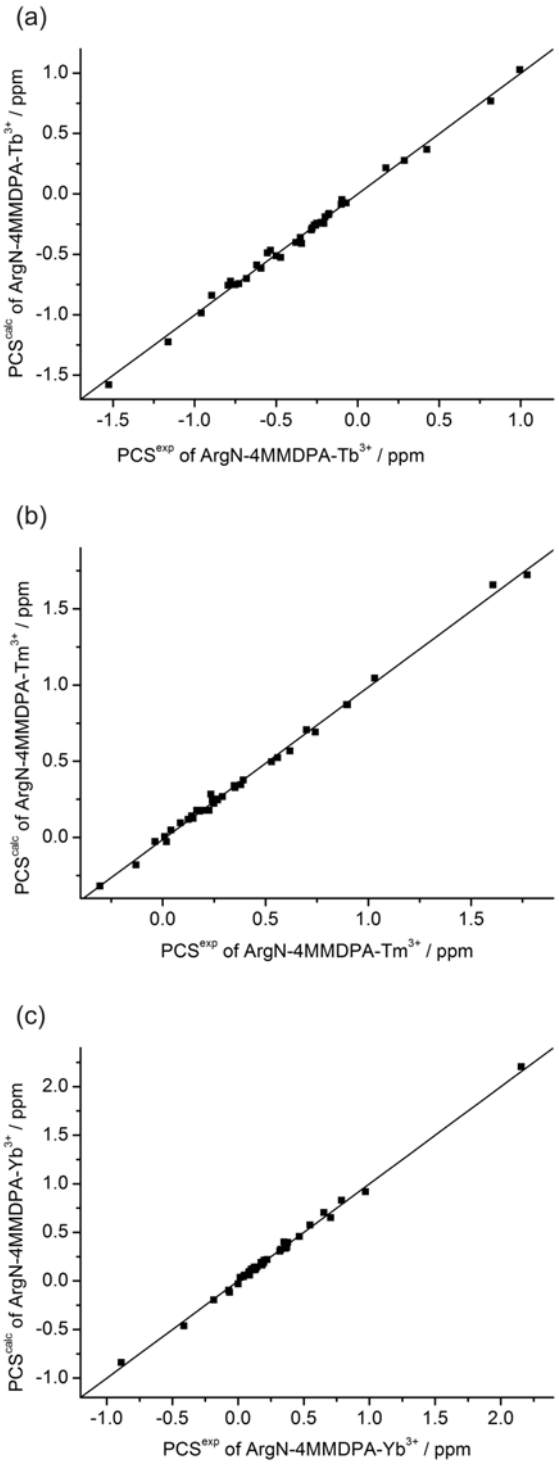

Figure S6. Plots of back-calculated PCS (PCS^{calc}) versus experimental PCS (PCS^{exp}) of backbone amide protons. PCS of residues 10-66 (Table S1) were used together with model 1 of the PDB coordinates 1AOY to represent the conformation of the ArgN-4MMDPA molecule. For visual guidance, a line of slope 1 has been drawn. (a) ArgN-4MMDPA-Tb^{3+} complex. (b) ArgN-4MMDPA-Tm^{3+} complex. (c) ArgN-4MMDPA-Yb^{3+} complex.

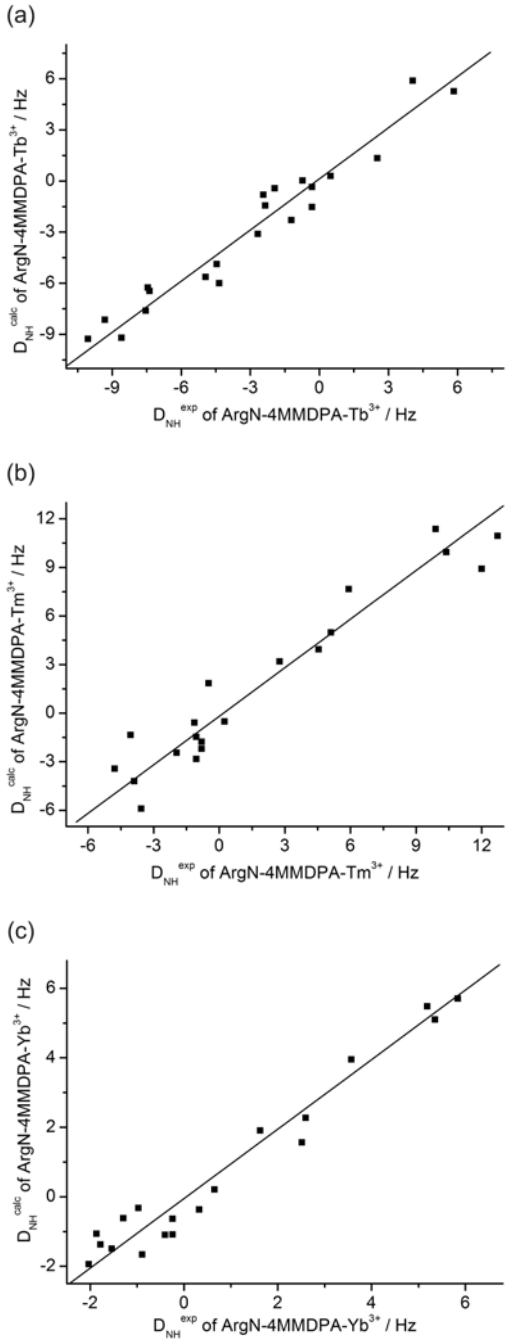

Figure S7. Plots of back-calculated RDCs (D_{NH}^{calc}) versus experimental RDCs (D_{NH}^{exp}) for backbone amides. Only data from regular secondary structure elements were included (see footnote b of Table S3), using model 1 of the PDB coordinates 1AOY to represent the conformation of the ArgN-4MMDPA molecule. The alignment tensors were those of Table S3. For visual guidance, a line of slope 1 has been drawn. (a) ArgN-4MMDPA-Tb^{3+} complex. (b) ArgN-4MMDPA-Tm^{3+} complex. (c) ArgN-4MMDPA-Yb^{3+} complex. The correlation plots of the RDCs are noisier than those of the PCS partly because RDCs are more sensitive to erroneous bond orientations than PCS and because RDCs are more difficult to measure accurately. Neither RDCs nor PCS had been used in the structure determination of ArgN.